Final report of AOARD-11-4015

"**Plasma metamaterials for arbitrary complex-amplitude wave filters**"

Osamu Sakai
Department of Electronic Science and Engineering, Kyoto University

Report Documentation Page

Form Approved
OMB No. 0704-0188

1. REPORT DATE	2. REPORT TYPE	3. DATES COVERED
10 SEP 2013	**Final**	**18-04-2011 to 17-04-2013**

4. TITLE AND SUBTITLE
Plasma metamaterials for arbitrary complex-amplitude wave filters

5a. CONTRACT NUMBER
FA2386-11-1-4015

5b. GRANT NUMBER

5c. PROGRAM ELEMENT NUMBER

6. AUTHOR(S)
Osamu Sakai

5d. PROJECT NUMBER

5e. TASK NUMBER

5f. WORK UNIT NUMBER

7. PERFORMING ORGANIZATION NAME(S) AND ADDRESS(ES)
Department of Electronic Science and Engineering,Kyoto University ,Kyoto-daigaku Katsura, ,Nishikyo-ku, Kyoto 615-8510, Japan,NA,NA

8. PERFORMING ORGANIZATION REPORT NUMBER
N/A

9. SPONSORING/MONITORING AGENCY NAME(S) AND ADDRESS(ES)
AOARD, UNIT 45002, APO, AP, 96338-5002

10. SPONSOR/MONITOR'S ACRONYM(S)
AOARD

11. SPONSOR/MONITOR'S REPORT NUMBER(S)

12. DISTRIBUTION/AVAILABILITY STATEMENT
Approved for public release; distribution unlimited

13. SUPPLEMENTARY NOTES

14. ABSTRACT
Investigations of arbitrary complex functions for electromagnetic waves by using a plasma array reinforced with metallic components and changing external discharge parameters, and their application to metamaterial-induced transparency of a plasma layer (ITEM 0001). Exploratory application of these investigations to high-power microwave control by plasma metamaterials (ITEM 0002).

15. SUBJECT TERMS
Metamaterials, plasma, complex-amplitude, wave filter

16. SECURITY CLASSIFICATION OF:			17. LIMITATION OF ABSTRACT	18. NUMBER OF PAGES	19a. NAME OF RESPONSIBLE PERSON
a. REPORT	b. ABSTRACT	c. THIS PAGE			
unclassified	**unclassified**	**unclassified**	**Same as Report (SAR)**	**53**	

Agenda of AOARD-11-4015

Project name

"Plasma metamaterials for arbitrary complex-amplitude wave filters"

Name of Principal Investigator

Osamu Sakai, Dr.

e-mail address :	osakai@kuee.kyoto-u.ac.jp
Institution :	Department of Electronic Science and Engineering, Kyoto University
Mailing Address :	Kyoto-daigaku Katsura, Nishikyo-ku, Kyoto 615-8510, Japan
Phone :	+81-75-383-2289
Fax :	+81-75-383-2290

Name of Program manager

Dr. Gregg H. Jessen and Dr. Matthew S. Zickafoose

Goal of this project

Investigations of arbitrary complex functions for electromagnetic waves by using a plasma array reinforced with metallic components and changing external discharge parameters, and their application to metamaterial-induced transparency of a plasma layer (ITEM 0001). Exploratory application of these investigations to high-power microwave control by plasma metamaterials (ITEM 0002).

I. Introduction

A plasma with hypothetically infinite size is a kind of media for electromagnetic waves, and their dispersion relations in various plasmas have been extensively studied.[1-3] Several schemes of plasma production and heating using the waves have been proposed and investigated experimentally and numerically; plasmas for fusion experiments as well as processing plasmas are controlled using launching antenna and high-power wave sources. One of the fundamental facts we have learned in microwave plasmas is that microwaves cannot usually propagate in an overdense plasma, which has a higher electron density n_e more than the cutoff density. To eliminate this phenomenon for achievement of high-density plasmas, we have to use external magnetic fields to modify the dispersion relation around the electron plasma frequency ω_{pe}, at which n_e reaches the cutoff density. When we use permittivity ε

and refractive index N for description of wave propagation, the reason why the wave cannot propagate in an overdense plasma is that N is imaginary since ε is negative, via the equation in the textbook $N=\sqrt{\varepsilon}$, when the wave angular frequency ω is less than ω_{pe}.

Such a negative ε state of plasmas is useful when we use plasmas for control of electromagnetic waves. Here, the waves do not necessarily propagate inside a plasma. Several authors reported effects from several viewpoints on such constituent plasmas as reflectors,[4] absorbers,[4,5] and antennae[6] of electromagnetic waves. In contrast with the other materials in these devices, parameters of the plasmas are fairly flexible to be adjusted, and its existence itself is controllable. Due to the limitation of available n_e in the devices, the frequency of the target waves is up to THz waves so far, although this limitation can be removed by forth-coming scientific and technological progresses.

Recently, after the proposal of their concepts,[7] metamaterials[8,9] have attracted much attentions to exhibit extraordinary features such as negative refractive index,[10] perfect lens effects,[11,12] and cloaking.[13] Here, states with negative ε are quite important to make N negative, via the formalism used in the metamaterial area $N=\sqrt{\varepsilon}\sqrt{\mu}$ and with a negative-μ state, where μ is (macroscopic) permeability, and are inevitable for elaborate control of N for cloaking. In an adjacent scientific area, plasmonics devices[14] which are composed of metals for light control in optics also utilize the negative ε states, in which surface plasmon polaritons are excited on the metal surfaces. In the area of industrial application of plasma processing, states with negative ε are effective for large-area plasma generation by surface waves, leading to relatively high n_e,[15,16] and other possibilities can be expected for future wave controllers.

This report demonstrates such recent progresses of wave controllers composed of plasmas and other materials, stimulated by the expanding researches of metamaterials. However, although the technique to realize negative-μ states is introduced from the proposal in the metamaterial area,[7] other unique characteristics that have not been observed in that area are found and shown here. So far, after the previous researches of a wave controller on the microstrip line[17,18] and photonic-crystal-like structures,[17,19-24] we reported effects of negative-ε plasmas in theoretical studies on localized surface-wave modes in chain structures of microplasmas,[24-26] and dynamic negative-N materials composed of plasmas and metallic resonators.[27,28] The entire area of our researches is summarized as "plasma metamaterials."[29]

In this report, we demonstrate the functional composites of plasmas and metamaterials, and the focusing point is verification of features on negative-ε plasmas previously predicted by our studies. The distinguished point from the ordinary

metamaterial researches, reported here, is the fact of flexible and complex negative ε as well as nonlinearity.[30]

II. Result 1: Arbitrary complex functions for electromagnetic waves by using a plasma array reinforced with metallic components (ITEM 0001)

States with negative ε, which we can achieve using plasmas and can be reinforced by metamaterials, are quite useful for flexible waveguides for microwaves. Here we confirm effects of negative ε in composites of gaseous plasmas and solid-state metamaterials, whose potential roles are wave controllers which can regulate attenuation and phase shift independently.

To detect a rapid change of complex-value scattering (S) parameters, both waves incident into and transmitted from a device under test (DUT) are monitored with good time response faster than the characteristic time of its dynamic properties. Furthermore, since the S parameters are complex variables, a detector is required to extract changes of both their amplitude and phase. Here, we built up a detecting system using microwave devices which can be described in ramp circuit elements. This is similar to a network analyzer, but its time response is enough to trace dynamic changes of plasma parameters.

Figure 1 shows a microwave circuit designed for this purpose. All of the devices and coaxial cables are applicable to microwaves up to 18 GHz. A signal generator (Agilent Technology, 83624B) provides microwaves at frequencies swept gradually, although the frequency was kept constant for time-varying DUTs. Incident microwaves are split into a probe wave and a reference wave, where the probe wave proceeds to a DUT and the reference wave directly goes to the S_{21} detector; the reference wave gives the invariant measure both in amplitude and phase components. A reflected wave from the DUT is also

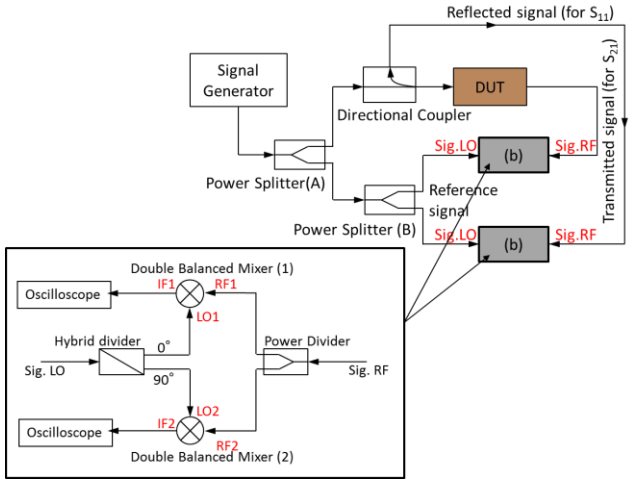

Fig. 1. Microwave circuit used for dynamic scattering parameters S_{11} and S_{21}.

detected at S_{11} detector through the directional coupler.

To detect a wave signal as a complex value, both S_{11} and S_{21} signals are filtered in a hybrid divider, in which a wave is split into two waves and one of them suffers phase shift of 90 degrees; using the signals in phase and in quadrature phase, we can derive both amplitude and phase components of the wave. We refer to this technique as In-phase Quadrature-phase (IQ) method in this article. We note that a conventional network analyzer has a processor unit that derives amplitude and phase of a wave signals;[39,40] the unit supports precise measurement for a various DUT, but requires some processing time which makes it difficult to catch up with dynamic change of DUT. The experimental results shown later in this article cannot verify its applicability for *every* DUT, although it works well for our DUTs, i.e., with $-4 \le \mathrm{Re}(N) \le 4$, $0 \le \mathrm{Im}(N) \le 5$, and a dynamic property with the characteristic time more than 0.1 μs.

As usually performed in a network analyzer, a calibration method to minimize error signals is required; the measurement plane at each port of a two-port device is not always the reference plane due to connection with series and parallel floating impedance. We performed this procedure according to the literature.[39,40] Furthermore, another error originates from multi reflection on the interface planes at the DUT front and end, which is observed as periodic humps along the frequency axis. This type of errors can be removed through series Fourier and Inversed-Fourier transform procedure; changing time evolutions to the frequency domain and removing fixed error spectra, we obtained pure signals coming from the source. The entire procedures were checked out using devices and waveguides whose properties were well known, and we could confirm that detected signals were sufficient for physical analysis at frequencies ranging from 2 to 7 GHz.

To prepare for a specific DUT, two spiral wires covered by insulator layers formed a double-helix structure, which leads to series inductance-capacitance resonance, and its array work macroscopically as a negative-permeability material if it has an external short-cut path and its loss component is negligibly small.[27, 28] We note that size of its outer diameter was 1.4 mm, much smaller than the wavelength of the microwaves at 7 GHz (~43 mm in the free space). The two insulated wires simultaneously worked as an electrode of a dielectric-barrier discharge. Since they were installed in a glass capillary which held a He or Ne flow, plasmas at elevated gas pressure were generated inside and outside of the double-helix structure. These plasmas made ε a complex value whose real part could be negative if n_e was so high that ω_{pe} was well beyond ω. This array composed of 15 units with its length of 30 mm was put on the surface of a coplanar waveguide with the length around 60 mm, and here we consider this coplanar waveguide with the array as a DUT. Both ends of the coplanar waveguide were

connected to the microwave circuit shown in Fig. 1 via coaxial connectors. Detailed installation and configuration of the DUT is shown in Fig. 2. Since the array of the metamaterial was coupled with electric and magnetic fields of the propagating microwaves on the coplanar waveguide, the electric fields are approximately parallel to the glass capillaries.[27,40] More rigorously, in this setup, we do not expect propagation of surface waves but performances as macroscopic media emerging in composites of plasmas and metal structures. The discharge voltage applied on the wired electrodes was operated at 5 kHz, and so this component which might affect the microwave waveguide could be removed by bias-T devices set on both sides of this DUT.

We performed experiments of microwave transmission through this DUT using the microwave circuit described earlier. A. In addition to the simple negative-ε effects, by varying gas conditions and electric power for plasma generation to control $\mathrm{Im}(\varepsilon)$ simultaneously and independently with $\mathrm{Re}(\varepsilon)$, we will see the entire properties of plasmas with negative-μ metamaterials. Note that μ determined by the double helix metal wires took a negative value just above magnetic resonance frequencies and a positive value outside the resonances; [28] one of the magnetic resonance frequencies was around 4.29 GHz. We here note smallness of the value of $|S_{21}|$ (~ 0.1) of this DUT in the following. Since we set the working point with negative μ, the DUT includes significant loss by enhancement of $\mathrm{Im}(N)$; outside magnetic resonances, $\mathrm{Im}(N)/\mathrm{Re}(N) < 0.05$, whereas $\mathrm{Im}(N) \sim \mathrm{Re}(N)$ without plasmas at 4.29 GHz around which $\mathrm{Re}(\mu)$ is negative, mainly due to large $\mathrm{Im}(\mu)$. One might suggest that large $\mathrm{Im}(\mu)$ will arise from extraordinary radiation losses, but we did not see such signs in measurements using a scanned micro monopole antenna around the DUT and the waveguide; radiation signals were several times lower when we installed this metamaterial structures on the coplanar waveguide around the frequency of negative μ, and we conclude that such a loss took place inside the metamaterial structure. This loss is inevitable when we use inductive-capacitive resonances,[9] although lossless magnetic resonances using dielectric resonators[40] can be applied to future plasma metamaterials.

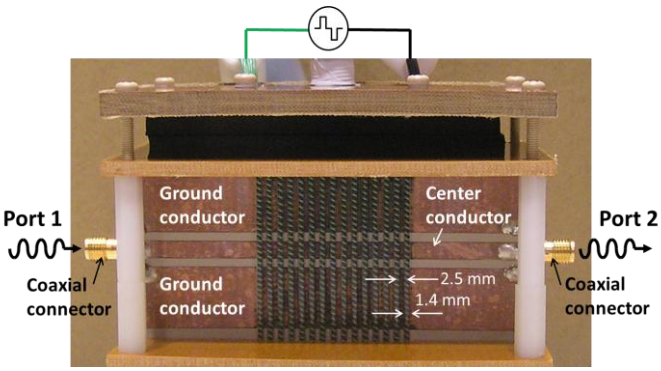

Fig. 2. Photo of DUT used in experiments.

Microscopic profiles of electric and magnetic fields are

complicated in similar manners to those in usual metamaterial experiments,[9] and we cannot specify detailed propagating modes on the coplanar waveguide with the DUT using a simple and conventional technological term. However, since the fundamental mode on the coplanar waveguide have electric fields which are almost parallel to the capillaries and perpendicular to the spiral wires, the electric fields mainly suffer plasma effects. On the other hand, the magnetic fields resonate with the wires at 4.29 GHz via the inductance-capacitance resonance. As a whole, effective macroscopic parameters of the media are determined through such plasma metamaterial effects, and can be analyzed by S_{21} and S_{11}.[9,43]

Specifically, we used He and Ne gases to control the working point significantly on the $\mathrm{Re}(\varepsilon)-\mathrm{Im}(\varepsilon)$ complex plane. He and Ne have different cross sections of elastic collisions,[44] by changing gas pressure, we can change the working point of ε on the plane. Note that the generated plasmas described here are collisional to see the effects of the varying working points on the complex plane; surface wave propagation, which is possible in collisionless plasmas as shown in Section III, can be ruled out.

In the case of He at atmospheric pressure (100 kPa) near the resonance (at 4.297 GHz), we showed the results of time evolutions of the discharge signals in Fig. 3. Using the signal of phase and amplitude of S_{21} in this time evolution and extracting the first phase of the discharge voltage in Fig. 3, we can make a new drawing of the varying working point of S_{21} on the complex plane in Fig. 4(a). The plasmas were generated in a scheme of dielectric barrier discharge. From Fig. 3, we recognized that the maximum n_e was observed just after the rising time of the discharge voltage (t ~ 5 μs), and that n_e decreased monotonously until the falling time of the discharge voltage (t ~ 20 μs); the axis of t can be converted to n_e. That is, such new drawings reveal dynamic and tunable properties of this metamaterial, which are expressed by the relation among three variables: $|S_{21}|\cos(\arg(S_{21}))$, $|S_{21}|\sin(\arg(S_{21}))$ and n_e.

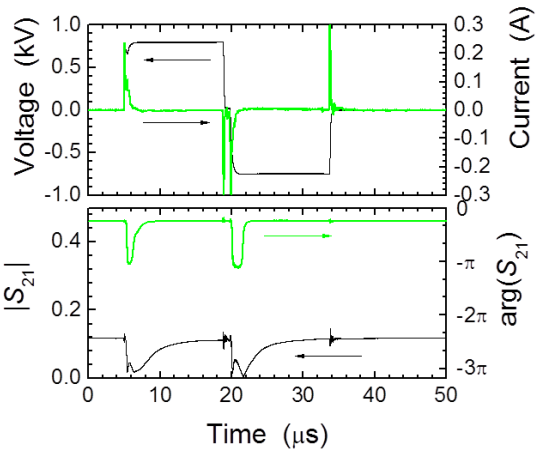

Fig. 3. Time evolutions of S21 and discharge signals in DUT at 100 kPa of He.

In Fig. 4(a), the trajectory was along one straight line on the plane, which indicates attenuation of the waves

took place without phase shift. Also shown in Fig. 7(a), plasmas are equivalently attenuators against microwaves in almost all cases except those shown in Fig. 8(b) and (c); electron collisions against neutral particles leads to $\mathrm{Im}(\varepsilon)$, which may result in $\mathrm{Im}(N)$.

Figure 4(b) shows varying S_{21} on the complex plane in the case of He at lower pressure (27 kPa) near the resonance (at 4.297 GHz). This case, we observed a similar trajectory to that in Fig. 4(a), but some swings due to phase shift was slightly found. In contrast, Fig. 4(c) shows varying S_{21} on the complex plane in the case of Ne at lower pressure (27 kPa) near the resonance (at 4.297 GHz). We observed clear phase shift in the time evolution, which means a significant change of $\mathrm{Re}(N)$ occurred. Furthermore, if μ, which is determined not by plasmas but by the double helix metal wires, changes to the positive value, the result is totally different; Fig. 4(d) shows S_{21} on the complex plane in the case of Ne at lower pressure (20 kPa) outside the resonance (at 6.0 GHz), and we can see only attenuation without significant phase shift.

These properties observed in the experiments include the DUT, the coplanar

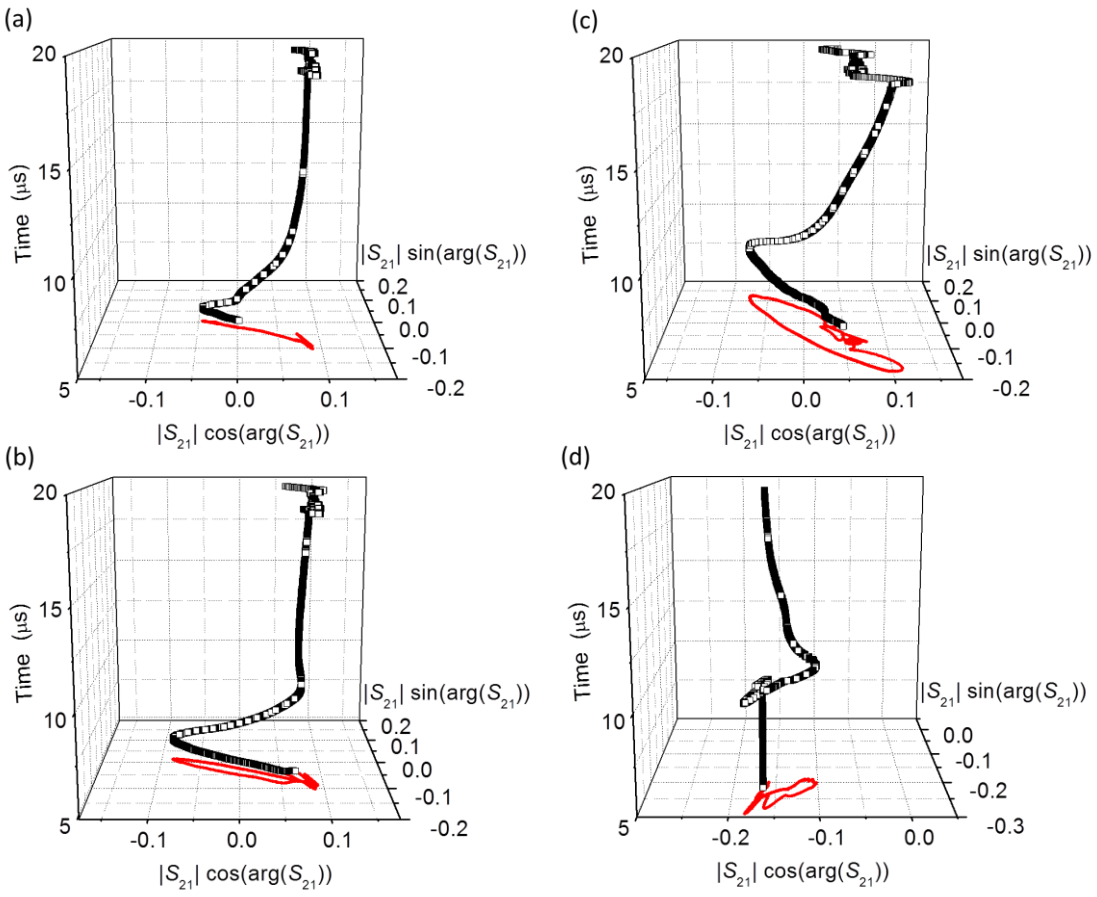

Fig. 4. Time evolutions of S21 on complex plane. (a) Near resonance at 100 kPa of He. (b) Near resonance at 27 kPa of He. (c) near resonance at 20 kPa of Ne. (d) Off resonance at 27 kPa of Ne.

waveguide, and the space on the upper side of the DUT. To derive macroscopic parameters of the metamaterial installed on the upper side of the DUT, we adapted one theoretical model developed for layered permittivity structure.[29,45] In Fig. 4(c), more than a 2π rad. swing of the trajectory was observed. Taking account of the fact that the length of the DUT was ~38 mm, it is concluded that $\mathrm{Re}(N)$ of the metamaterial, the composite of the plasmas and the magnetic resonators, reached $-1.5--3$ when the maximum phase shift took place; a dynamic negative-N material was successfully observed.

Here, we mention about variation of such macroscopic parameters depending on gas conditions and μ. Figure 5 displays n_e dependence of ε.[23,28,29,46] As the collisional frequency becomes lower, both changes in $\mathrm{Re}(\varepsilon)$ and $\mathrm{Im}(\varepsilon)$ get larger. On the other hand, higher collisional frequency makes the ratio $\mathrm{Im}(\varepsilon)/\mathrm{Re}(\varepsilon)$ larger. Similar tendencies are found for $\mathrm{Re}(\sqrt{\varepsilon})$ and $\mathrm{Im}(\sqrt{\varepsilon})$. These facts indicate that the change of electron elastic collisions by selection of gas species and pressure leads to wave attenuation and phase shift, which are controllable independently. Furthermore, due to the rotation of the working points on the complex $\sqrt{\varepsilon}$ by product with $\sqrt{\mu}$, variation of n_e makes either change of $\mathrm{Re}(N)$ or $\mathrm{Im}(N)$;[46] this is one of the unique features predicted for plasma metamaterials, and was verified in Fig. 4 (c) and (d). Simultaneous realization of flexible waveguides and variable attenuators with controllable phase shifts is not shown in this report, but it will be possible in future schemes of localized surface wave propagation on negative refractive index materials[47] composed of plasmas.

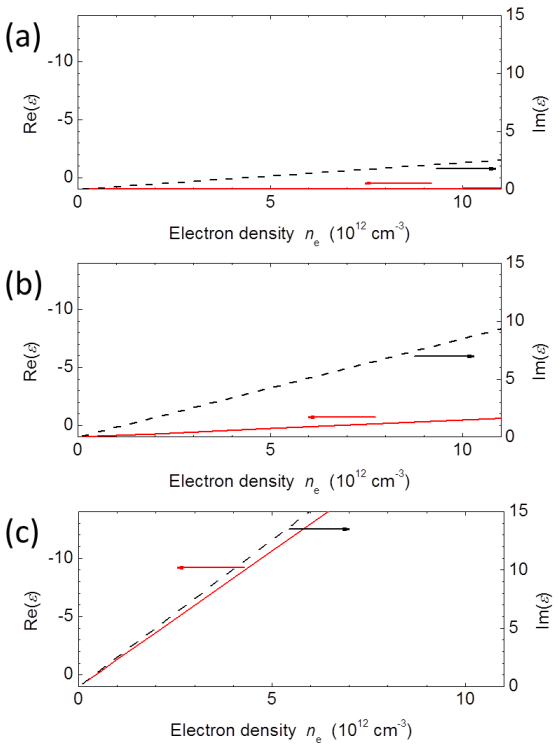

Fig. 5. Complex permittivity ε as a function of electron density n_e. (a) He at 100 kPa. (b) He at 27 kPa. (c) Ne at 20 kPa.

III. Result 2: Metamaterial-induced transparency of plasma layer (ITEM 0001, 0002)

When we arrange microplasmas around 1 mm along one line on one plane, microwaves with its frequency slightly less than ω_{pe} can propagate along this chain strucrture,[24,25] similar to localized surface plasmon polaritons.[14] Since microwaves form standing waves around an individual microplasma in a microscopic point of view, we expect that the waves can propagate along bent or diverged chains, changing the direction of its macroscopic wave vector.

A. Numerical analysis of propagating localized surface waves in various patterns of plasmas

When we arrange microplasmas around 1 mm along one line on one plane, microwaves with its frequency slightly less than ω_{pe} can propagate along this chain strucrture,[24,25] similar to localized surface plasmon polaritons.[14] Since microwaves form standing waves around an individual microplasma in a microscopic point of view, we expect that the waves can propagate along bent or diverged chains, changing the direction of its macroscopic wave vector.

First, we performed numerical analysis to confirm these predictions. The method we used was different from the one for derivation of dispersion relation in an infinite periodic structure;[24] the finite difference time domain (FDTD) method for dispersive media in the Drude model was applied to study this phenomena, since it can deal with finite and specific structures. Its formalism was described in our previous report,[23] and the essential point is that we introduced one extra equation for balance of current densities of microwave fluctuations in addition to the Maxwell equations. We investigated in-plane electric-field modes which have electric fields parallel to the calculated two-dimensional plane with perpendicular magnetic fields.[21,24,31] We assumed that microwaves are launched by a micro dipole antenna, which is given by a FDTD cell with fixed electric field in the direction of the y axis near the plasma column on the edge and clarifies the coupling point to that plasma; port analysis for scattering matrix is not performed.

Figure 6 shows a case of a simple straight chain of microplasma columns with microwave launching points and calculated electric fields expressed by their amplitudes. We assumed radial distribution of n_e in the usual zero-order Bessel function J_0 in the model, where it is monotonous with peaking in the center and boundary condition of $n_e = 0$ on the edge. The exposed electric field has an y component E_y with no x

component E_x, and this E_y works for a boundary condition of the Maxwell equations and a source for near field in the y direction. The calculated results shown in Fig. 6(b) and (c) indicated that electric fields are localized on the edge of the plasmas, and propagate along the chain structure, as described in the following. Since the excitation point is very close to the first microplasma column, the excited E_y near fields induce surface waves on the round surface of this plasma column, where the surface waves have electric field components parallel to and perpendicular to a round interface between a positive ε layer (outside region) and a negative ε layer (inside plasma region).[3,32,33] The surface waves propagate around this surface, changing its propagation direction and its field components as mixtures of E_y and E_x that are symmetrical in magnitude. When they go to the other end of the round surface of the first plasma column, another microplasma column is just in front of them; most of the wave energy is coupled to surface waves on the next microplasma column. From macroscopic points of view, the exposed E_y near field on the bottom edge of the column chain excites wave propagation along the chain in the y direction. There are very little component of propagating (plane) waves excited from the antenna and directly coupled to the plasma columns, because an excited propagating wave has a Poynting vector in the x direction. The maximum value of $n_e (= 1.5\times10^{13}\ \mathrm{cm}^{-3})$ in the center of the individual plasma corresponds to the local electron plasma frequency ~34 GHz. That is, the excited wave frequency (13.1 GHz) is well below the cutoff density and the wave cannot propagate inside the bulk region. The value of ε reaches $-20--30$ in the center, and that on the region of localized electric fields of the surface waves is $0--1$, which are suitable for surface wave propagation on interface between the positive ε layer (outside region) and the negative ε layer (inside plasma region).

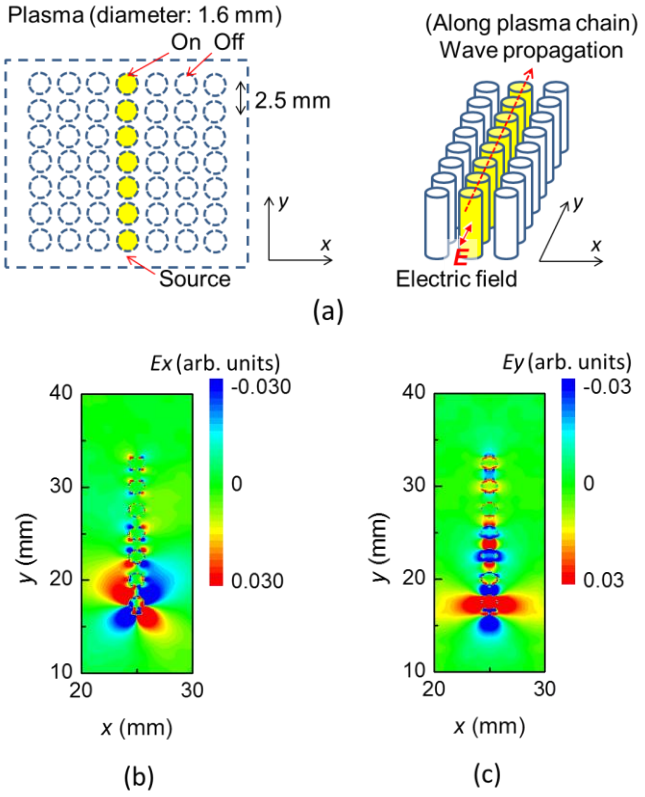

Fig. 6. (a) Numerical model of straight plasma chain used here. (b) E_x at 13.1 GHz calculated numerically. (c) E_y at 13.1 GHz calculated numerically.

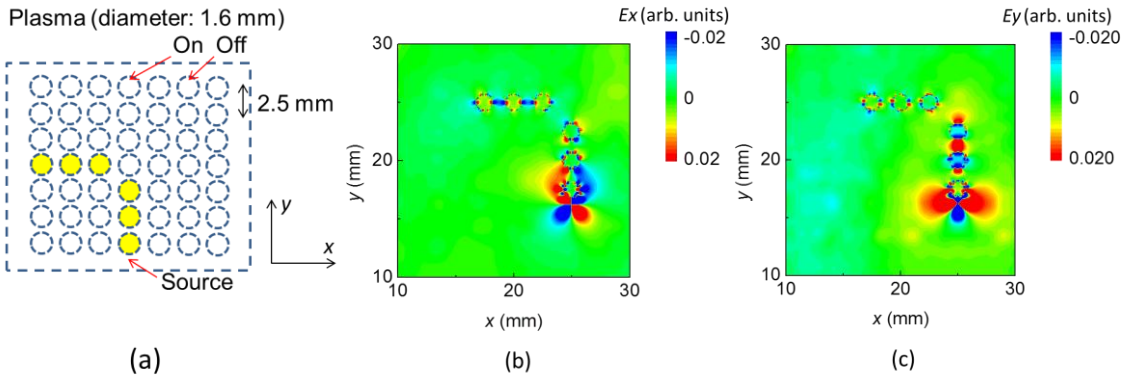

Fig. 7. (a) Numerical model of L-like-angled plasma chain used here. (b) E_x at 13.1 GHz calculated numerically. (c) E_y at 13.1 GHz calculated numerically.

Figure 7 shows wave propagation along an L-shaped bent line of the chains. The wave successfully changes its propagation direction along the plasma chain. Such a bent propagation path is possible since the wave propagates microscopically along the edge of an individual plasma and partially jumps to the adjacent plasma through a sneaking component normal to the plasma surface. Note that the wavelength of the surface wave is much shorter than propagating waves in free space due to its resonance property. We previously reported a T-junction of similar plasma chain structures,[29] and these facts indicate that such waveguides can be designed only with plasma chain structures.

B. Experimental observation of localized surface waves and their propagation

To verify the prediction of the numerical results shown earlier, we performed experiments in the similar situation of the numerical model. We generated columnar plasmas with sufficiently long length (~ 36 mm) in capillary-shaped holes in a dielectric cube (teflon, ε ~2.1). Using Ar gas at 500 Pa, we generated plasmas by pulsed low frequency waves at 370 kHz whose amplitude reached around 0.8 kV. The gas pressure we set assures that plasmas generated here are almost collisionless, which means that $\mathrm{Re}(\varepsilon)$ varies with almost no change of $\mathrm{Im}(\varepsilon)$.

Figure 8(a) displays visible emissions from the generated plasmas, viewed from one end of the capillary; one end was a mesh electrode to pass the emission light and assure the flat grounded potential profile. The plasmas were well confined in each capillary without any leakage, and formed a straight line composed of seven ignited columns; plasmas were not generated in other surrounding capillary holes. Now, two

micro monopole antennae, both of which were directed in the y axis in Fig. 1(a), were set at both ends, and one was for the launcher of microwaves supplied from a signal generator (Agilent Technology, 83624B), and the other was the receiver with a rectifier to monitor the amplitude of the wave. The launcher antenna is a micro monopole antenna with the length of 1 mm on a microwave coaxial cable, which enables us to assure similar plasma-field coupling to the numerical analysis shown Fig. 6 and 7; it emits a sufficient component of electric near fields in the direction of y axis. Figure 8(a) also shows a detected signal profile when the transmitted signal was fairly strong (at 1.51 GHz). Its profile was quite similar to the electric field distribution at the end of the chain calculated numerically, as shown in Fig. 6, for example. If the receiver signals came from the propagating plane waves in the y direction, we could detect almost no signals since the launcher and the receiver antenna mainly had a E_y component, but it was not the case at this frequency. Surface waves numerically investigated in Figs. 6 and 7 have electric fields of both x and y components,[3,32,33] and the detected E_y electric fields are consistent with this predicted features.

Figure 8(b) shows frequency spectra of the transmitted waves. Such multiple peaks of the spectrum in "enhancement factor", which is defined as the ratio of signals between those with and without plasmas, were quite similar to the dispersion relations predicted previously.[24,25,29] That is, spectra without plasmas indicate microwave propagation through the dielectric with periodic capillary tubes, and spectrum variation found in those with plasmas in comparison

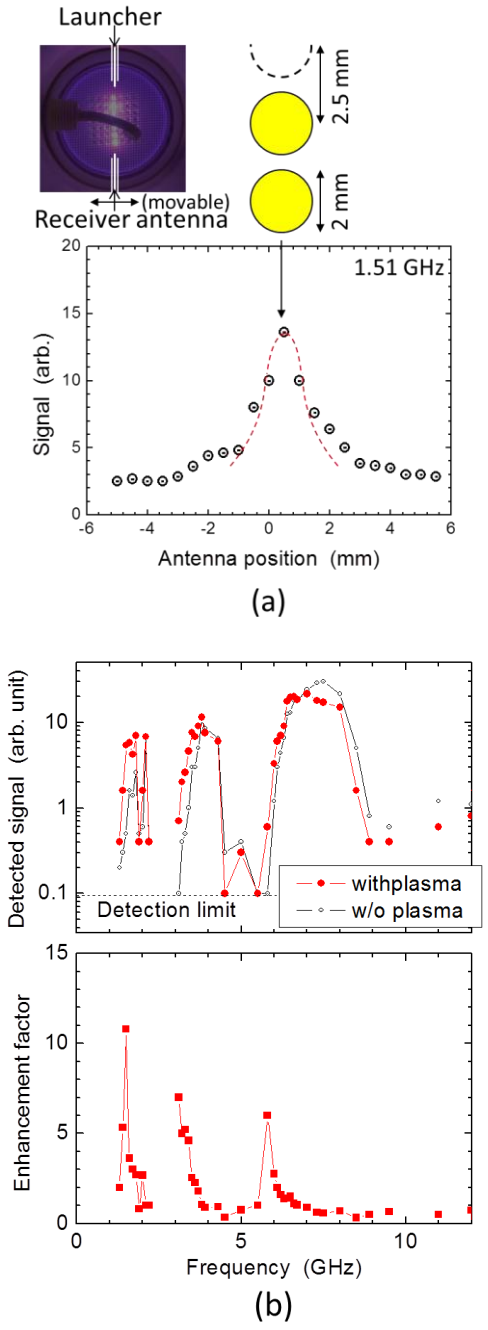

Fig. 8. (a) Spatial profile of detected electric field in straight plasma chain configuration. (b) Frequency spectra in similar configuration.

with the case without plasmas reflects microwave propagation along chain-like plasma columns. Among the observed spectra, we stress here that the spectrum around 1.5 GHz shows a very clear evidence of microwave chain-like propagation, as described in the following. The spectrum around 1.5 GHz in the case with plasma generation shows clear enhancement in signals of transmitted waves, whereas the signal is quite low in the case without plasma generation, although all the displayed signals in Fig. 3 are more than 10 times larger than the noise levels; the signals below the maximum noise level (< 0.1 in units of the y axis in Fig. 3) are omitted from the plotted data. On the other hand, other two peaks in the case with plasma generation above 2 GHz are very close to the peaking signals without plasmas, and confirmation of chain-like propagation is uncertain. This is partly because (plane) waves may propagate in free space in these higher frequencies; since we cannot complete ideal settings in all cases, especially in high frequency regions, the monopole antenna may excite waves with some components of propagation in the y direction, and such wave components will obscure signals of chain-like propagation. The intensity variation in the frequency spectra above 2 GHz may come from standing waves between the launcher and the receiver antennae. On the other hand, below 2 GHz, the signals in the cases without plasmas were so low, which indicates sufficient elimination of wave propagation in free space. In fact, in this frequency range, half-wavelength standing waves cannot exist due to short distance between the antennae (~ 20 mm); most of the detected signals in the cases without plasmas are expanding near-field ones. These facts support experimental confirmation of the similar waves predicted in the numerical models for the spectrum around 1.5 GHz. Another point we can understand from this data is that n_e might be lower than the cases investigated numerically; possible values of n_e would be the order of 10^{12} cm^{-3} with the maximum local values of $\omega_{pe}/2\pi$ = 10-20 GHz.

The enhancement factor shown in Fig. 8(b) is not always effective on quantitative estimation, and it is not equal to physical amplification rate due to the above mentioned influences of other signal mixing. However, from this factor, we can certainly recognize frequency spectra whose widths are quite small.

Note that such behaviors of surface wave propagation on negative-ε microplasma chains were not well investigated before this report. The surface waves localized on individual plasmas and connected to adjacent plasma(s) along the chain are different from near fields which are simply explained by the Poisson's equation and no sensitive dependence on wave frequency. Similar wave guiding effects have been reported as surface plasmon propagation on nano-metallic particle chains[14, 34-38], but they are in the photon range and with different spatial ε profiles. Here we show theoretical predictions on details of the surface waves on plasma chains and their

experimental evidences on localization both in space and frequency domain, which are only explained by propagation of such localized surface waves.

IV. Result 3: Exploratory application to high-power microwave control by plasma metamaterials (ITEM 0002)

When energy of propagating electromagnetic waves in a negative-permeability space becomes high, the waves generate plasmas, and the plasmas change electric permittivity in the corrresponding space; this is a nonlinear evolution, and should be treated in a self-consistent analysis. Here, we investigated such an effect theoretically and experimentally, and they generated overdense plasmas successfully and part of the microwaves can transmit in a nonlinear scheme. Theoretical analysis predicts that high-density plasmas with negative permittivity can form via saddle-node bifurcations within an adequate electric field. To confirm theoretical predictions, using metamaterials with negative permeability achieved by magnetic resonances, we inject microwaves with several hundreds of watt into a waveguide filled with low-pressure discharge gases, and we confirmed transmission of switchable high-power 2.45 GHz as well as overdense plasmas with negative permittivity.

A. Theoretical analysis of nonlinear system

To maintain complete self-consistency between the microwave energy and n_e in a generated plasma, numerical analysis including a fluid model with particle balance and Maxwell equations is preferred, but it is rather difficult to extract underlying physics since calculated results obtained in numerical analysis is fairly complicated. Here, we use the method reported by our group recently[30], reviewed briefly in the following. The electric fields of both propagating and evanescent waves at spatial position $\boldsymbol{r}$ and time t have phase terms including N, expressed using wavenumber $\boldsymbol{k}$ and frequency of the waves $\omega/2\pi$ is frequency of the waves. N is defined in regimes of metamaterials by μ, which is a macroscopic value determined by synthesized effects of array of metamaterial components, and ε, which is a microscopic value determined by collective motions of electrons in plasmas and given in the Drude model using electron plasma frequency ω_{pe}, vacuum permittivity ε_0, and electron mass m_e. We assume collisionless plasmas. If plasmas are generated by electric-field drift motions of electrons and recombined without spatial transport, electron continuum equation from

the particle balance expressed with electron mobility η_e and recombination coefficient β, which includes the terms of production rate and recombination rate. Ionization coefficient $¥alpha$ is expressed with two constants C = 29.2 and D = 26.6 for Ag gas[39] when we use α, p and E in the units of cm^{-1}, Torr and V/cm, respectively. In a steady state, n_e is as a function of E.

This system includes E, ε and n_e, and we solve this nonlinear system by comparing two plots of E as a function of ε at each spatial position. We use similar numerical results reported in Ref. 30. Then, we modify the parameter of Ar gas pressure to 100 Pa, which was different from that in Ref. 30 and similar in the experiments shown below, and calculate E. Finally, we will obtain bifurcation diagrams which indicate ε transitions when we change injection power of microwaves P_i or electric field at the source point E_i. Note that n_e is uniform in the metamaterial region with slight spatial modulation that reflects discrete unit structures in the metamaterials, and loss mechanisms of electrons are recombination in a given position at which they are generated.

First, we explain the model and the results of theoretical analysis using Fig. 9. Figure 9 (a) shows numerical model calculated by the finite difference time domain method. From the source, continuous sinusoidal waves at 2.45 GHz was launched, and the metamaterial region with 150×200 mm^2 had a specific μ = -1. ε and μ in the surrounding region are both unity. By changing ε in the metamaterial region, we can derive stable values of the local electric field. Note that near fields around the source point induce wave propagation inside the metamaterial region since the point source was so close to the region, by 10-mm distance.

Figures 9 (b) and (c) demonstrate examples of numerical results. When n_e is low and ε is positive (Fig. 9 (b)), N is imaginary since μ is negative. As a result, the waves cannot propagate inside the metamaterial region. On the other hand, when the plasma is overdense and ε is negative (Fig. 9

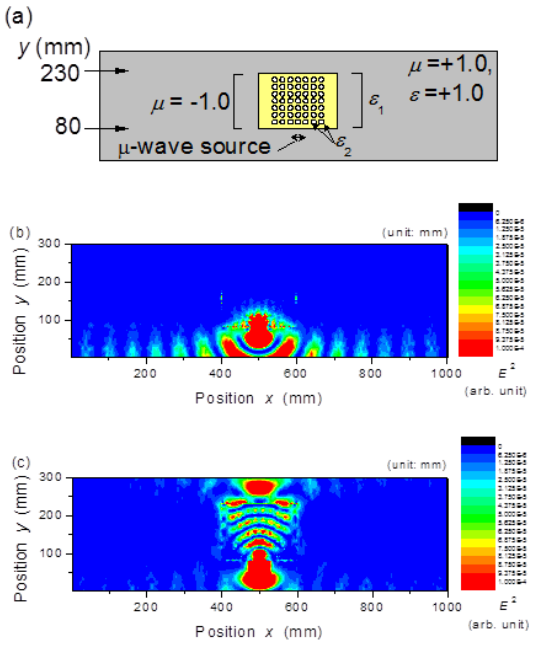

Fig. 9. (a) Numerical model used here. (b) Electric fields calculated numerically for ε = 0.2. (c) Electric fields calculated numerically for ε = -6.0.

(c)), they can propagate inside the region. These features are completely on the contrary to conventional cases with positive μ one of which is typically shown in Fig. 9 (b). When both ε and μ are negative, the phase velocity is reversed although the Poynting vector is forward from the wave source point .[29]

After calculation of wave propagation in various cases of ε, we obtained local electric fields E_n at several points along the propagation path. Figure 10 (a) shows the local electric fields calculated numerically. Due to the specific geometrical effects, we recognize data scattering irregularly, but roughly we can estimate dependence of the fields by solid curves as a function of ε. In all cases, the fields are almost the same when ε is fairly negative. On the other hand, at the points apart from the microwave source, we observe almost no electric fields when ε is positive. At the points that are very close to the microwave source, the fields are strong due to evanescent waves even in the cases with positive ε.

Electric fields are also calculated from the particle balance equation, shown as E_r in Fig. 10 (b). We note that E_n is expressed in the arbitrary unit and linearly depends on E_i. That is, to see variation of n_e and ε as a function of E_i, the solutions are given by crossing points of E_r, which are the fixed values, and E_n with varying E_i.

Figure 11 shows ε dependences on the electric field at the source point of microwaves E_i which is directly dependent on P_i. At the position of y = 100 mm, evanescent waves with near fields are dominant, and we observe only a small bifurcation around $\varepsilon \sim 0$ and hysteresis takes place with a small difference of E_i (0.3-0.4 in the arbitrary unit in Fig. 11). At the position of y = 120 mm, propagation waves join evanescent waves which are depressed as the position becomes apart from the edge of the metamaterial region. As a result, clearer bifurcations are

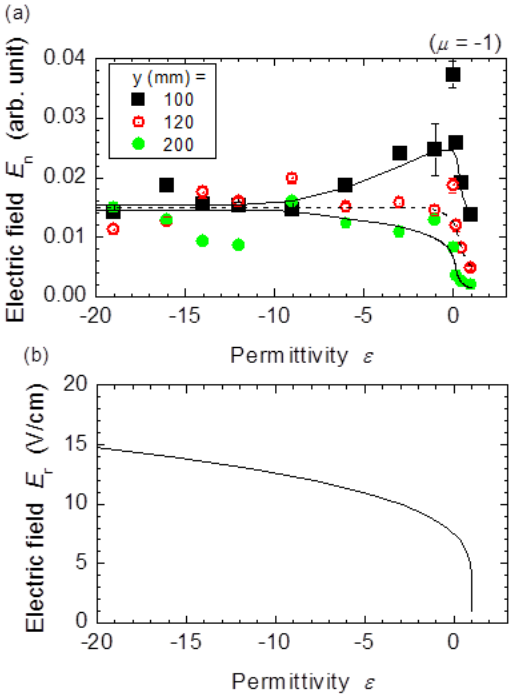

Fig. 10. (a) Electric fields calculated numerically on wave propagation for various ε. (b) Electric fields calculated analytically from paraticle balance for various ε.

observed, and two saddle-node bifurcation points at E_i ~ 1 and 0.6 can be recognized. That is, as the working point goes up to E_i ~ 1, ε remains around +1. Then, at the bifurcation point around E_i = 1, ε jumps up to ~ -20, which indicates high-n_e plasma generation with n_e ~ 10^{12} cm^{-3}. After the high-n_e plasma generation, as the working point goes down to E_i ~ 0.6, the plasmas are in overdense states with negative ε, and then, ε jumps down to ~ +1 around E_i = 0.6. In the case at y = 200 mm, around which the propagating waves are dominant, significant bifurcations with larger hysteresis are observed. In the cases at y = 120 mm and 200 mm, no plasma generation is expected at positive ε and the plasmas are always overdense.

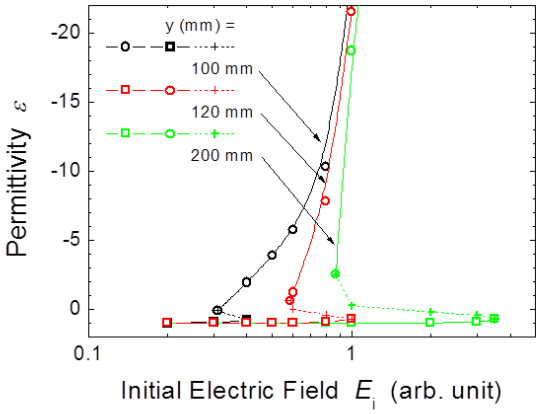

Fig. 11. Bifurcation diagrams between ε and initial electric field at microwave source.

B. Experimental verification of enhanced wave transmission and overdense plasma generation

To verify the above-mentioned theoretical predictions, we generated plasmas at low pressure using metamaterials with macroscopic negative μ. The experimental setup is shown in Fig. 12. The conventional rectangular waveguide at 2.45 GHz was installed in a vacuum chamber, which was filled with Ar at 100 Pa. This gas pressure assures generation of collisionless plasmas. We note that waveguide structure was almost kept both outside and inside the vacuum chamber, only with small discontinuity at the vacuum window made of quartz glass located at y = 0.

We set an array of double split ring resonators[7] as a negative-μ metamaterial for the region from y = 0 to 80 mm; it consisted of designed copper films via a wet etching process from plane copper-covered glass-epoxy substrates. By derivation of the scattering parameters with the vector network analyzer (Anritsu Corp., MS2028B) and using the parameter retrieval method,[43] we could evaluate the value of macroscopic μ. In the case in Fig. 12(b), the magnetic fields H penetrated the rings and we expected achievement of negative μ near their magnetic resonance, and μ was derived as -0.5-0.1j at 2.45 GHz. On the other hand, in the case in Fig. 12(c), the magnetic fields

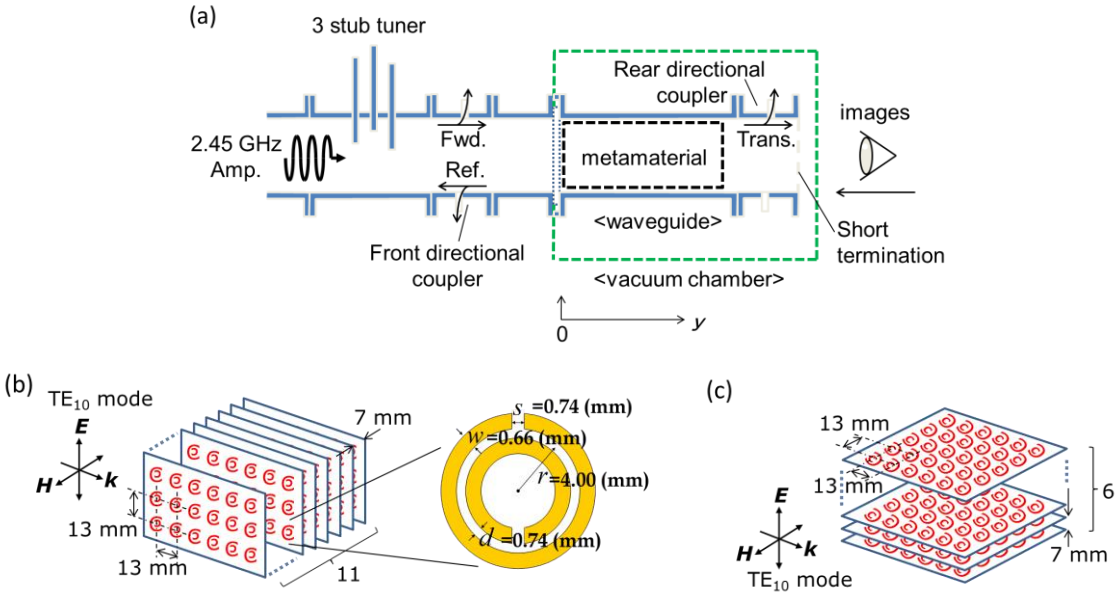

Fig. 12. (a) Experimental setup for high-power microwave injection into negative-μ metamaterial. (b) Metamaterial for negative μ. (c) Metamaterial for positive μ.

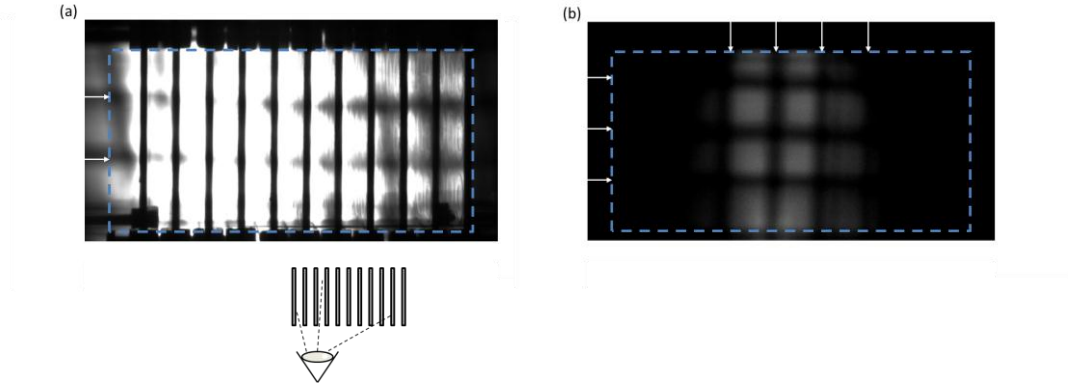

Fig. 13. (a) Visible image of plasma emission for negative μ. (c) Visible image of plasma emission for positive μ.

H never penetrated the rings and we could not expect negative μ since there were no magnetic resonances; as a result, μ was derived as ~ +1 at 2.45 GHz.

Then, we injected 2.45-GHz microwaves with 360 W as a forward power with 25-μsec width from a high-power microwave amplifier (Kyoto-Micro-Densi, MA-02400C) into the vacuum chamber. Figure 13(a) shows visible emission of plasmas generated in the metamaterial region of Fig. 12(b). The images seemed to be inhomogeneous due to the view angle, but they were uniform on the cross section of the metamaterial. From emissions near the right edge, we noticed that intensified emissions were near the entrance of the metamaterial region, and they decreases gradually as the microwaves propagated. In comparison, when we use another metamaterials structure, shown in Fig. 12(c), whose DSRRs are perpendicular to those in Fig. 12(b), we

observed very weak and unstable emissions as shown in Fig. 13(b). We note that we detect no signals above the detection limit of single Langmuir probes in the case shown in Fig. 12(c).

Now we are concentrated on results of the negative μ metamaterial shown in Fig. 12(b). Figure 14(a) shows time evolutions of transmitted power detected by the directional coupler on the other side of the entrance. Without plasma generation, we did not detect any signals, unlike the forward- and the reflected-power signals. However, when the plasmas were generated, the transmitted power was detected, as shown in Fig. 14(a), and *increased*; *this is the clear evidence for switchable passive microwave transmitters based on this plasma metamaterial configuration*. Such phenomena were not the case of microwave plasma generation in conventional schemes; usually, after plasma generation, the transmitted power decreases due to power dissipation. In our case, the change of N from the imaginary state with positive ε and negative μ to the real state with a double negative system induced enhancement of transmittance.

Figure 14 also shows ion saturation current I_{is} at bias voltage of -20 V measured by a conventional single probe at y = 10 mm; this signal coincided with the power signals. By changing bias voltage, we obtained probe current-voltage curves in a few tens of shots. Figure 14(c) shows evolution of n_e and electron

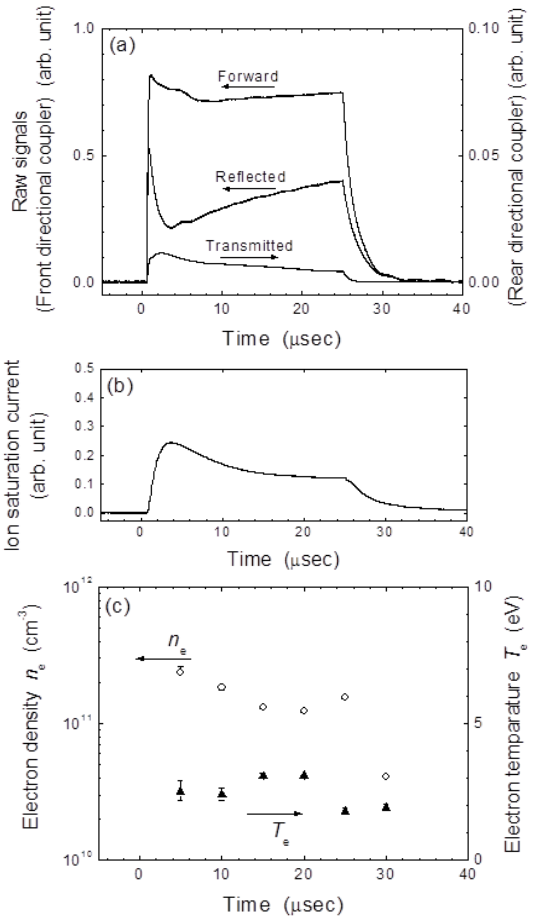

Fig. 14. Time evolutions of (a) microwave signals, (b) probe signal, and (c) plasma parameters.

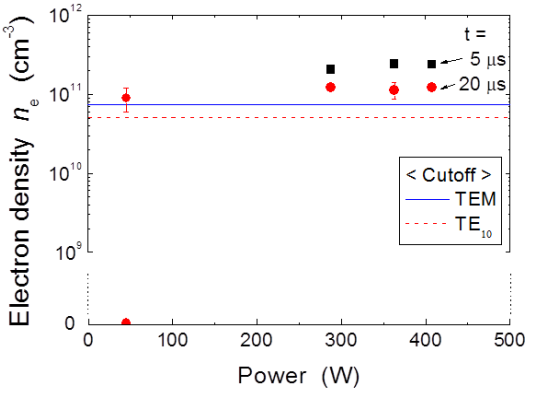

Fig. 15. Electron density n_e as a function of forward microwave power..

temperature T_e. The solid line indicates the well-known cutoff density (7.4×10^{10} cm^{-3}) for waves in the TEM mode or propagating in an infinite plasma, and the dashed line indicates the cutoff density (5.1×10^{10} cm^{-3}) for those in the TE_{10} mode or propagating in an plasma occupying the rectangular waveguide. Monitored n_e is always well beyond the both cutoff densities; overdense plasmas with negative ε were successfully generated.

Figure 15 shows variation of n_e as a function of the forward power P_f. When P_f was quite low (less than 40 W), we did not recognize any plasma generation, and when it was higher than 100 W, we always observed overdense plasmas. When P_f is around 50 W, we detected plasmas in some discharge shots and no plasmas in the other shots, and in the cases of plasma generation, we always observed overdense plasmas; we note that ε = 0 at the cutoff condition, which is in the TE_{10} mode since we generated plasmas inside the waveguide. This experimental results indicate two possible states, similar to bifurcated solutions of n_e or ε for E_i = 0.6-1.0 with 40 mm shown in Fig. 11.

V. References

[1] T. H. Stix, *The Theory of Plasma Waves* (McGraw-Hill, New York, 1962).

[2] V. L. Ginzburg, *The Propagation of Electromagnetic Waves in Plasma* (Pergamon, Oxford, 1964).

[3] D. G. Swanson, *Plasma Waves* (Academic, Boston, 1989).

[4] R. J. Vidmar, IEEE Trans. Plasma Sci. **18**, 733 (1990).

[5] Y. P. Bliokh, J. Felsteiner and Y. Z. Slutsker, Phys. Rev. Lett. **95**, 165003 (2005).

[6] G. G. Borg, J. H. Harris, N. M. Martin, D. Thorncraft, R. Milliken, D. G. Miljak, B. Kwan, T. Ng, and J. Kircher, Phys. Plasmas **7**, 2198 (2000).

[7] J. B. Pendry, A. J. Holden, D. J. Robbins and W. J. Stewart, IEEE Trans. Microw. Theory Technol. **47**, 2075 (1999).

[8] A. Sihvola (ed.), *Advances in Electromagnetics of Complex Media and Metamaterials* (Kulwer Academic Publishers, Dordrecht, 2002).

[9] L. Solymar and E. Shamonina, *Waves in Metamaterials* (Oxford University Press, Oxford, 2009).

[10] V. G. Veselago, Sov. Phys. Usp. **10**, 509 (1968).

[11] J. B. Pendry, Phys. Rev. Lett. **85**, 3966 (2000).

[12] R. A. Shelby, D. R. Smith, and S. Schultz, Science **292**, 77 (2001).
[13] J. B. Pendry, D. Schurig and D. R. Smith, Science 312 1780, Science **312**, 1780 (2006).
[14] S. A. Maier, *Plasmonics: Fundamentals and Applications* (Springer, New York, 2007).
[15] J. C. Nickel, J. V. Parker and R. W. Gould, Phys. Rev. Lett. **11**, 183 (1963).
[16] I. P. Ganachev and H. Sugai, Surf. Coat. Technol. **200**, 792 (2005).
[17] O. Sakai, T. Sakaguchi, Y. Ito, and K. Tachibana, Plasma Phys. Controlled Fusion **47**, B617 (2005).
[18] O. Sakai and K. Tachibana, IEEE Trans. Plasma Sci. **34**, 80 (2006).
[19] O. Sakai, T. Sakaguchi, and K. Tachibana, Appl. Phys. Lett. **87**, 241505 (2005).
[20] O. Sakai, T. Sakaguchi, and K. Tachibana, Contrib. Plasma Phys. **47**, 96 (2007).
[21] O. Sakai, T. Sakaguchi, and K. Tachibana, J. Appl. Phys. **101**, 073304 (2007).
[22] T. Sakaguchi, O. Sakai, and K. Tachibana, J. Appl. Phys. **101**, 073305 (2007).
[23] O. Sakai, T. Naito, and K. Tachibana, Phys. Plasmas **101**, 057102 (2010).
[24] O. Sakai and K. Tachibana, IEEE Trans. Plasma Sci. **35**, 1267 (2007).
[25] O. Sakai, T. Naito and K. Tachibana, Plasma Fusion Res. **4**, 052 (2009).
[26] O. Sakai, T. Sakaguchi, T. Naito, D.-S. Lee and K. Tachibana, Plasma Phys. Control. Fusion **49**, B453 (2007).
[27] O. Sakai, T. Naito, T. Shimomura and K. Tachibana, Thin Solid Films **518**, 3444 (2010).
[28] O. Sakai, T. Shimomura and K. Tachibana, Phys. Plasmas **17**, 123504 (2010).
[29] O. Sakai and K. Tachibana, Plasmas Sources Sci. Technol. **21**, 013001 (2012).
[30] O. Sakai, J. Appl. Phys. **109**, 084914 (2011).
[31] C. Luo, S. G. Johnson, J. D. Joannopoulos and J. B. Pendry, Phys. Rev. B **65**, 201104 (2002).
[32] A. W. Trivelpiece and R. W. Gould, J. Appl. Phys. **30**, 1784 (1959).
[33] K. Sakoda, N. Kawai, T. Ito, A. Chutinan, S. Noda, T. Mitsuyu, and K. Hirano, Phys. Rev. B **64**, 045116 (2001).
[34] J. R. Krenn, A. Dereux, J. C. Weeber, E. Bourillot, Y. Lacroute, J. P. Goudonnet, G. Schider, W. Gotschy, A. Leitner and F. R. Aussenegg, Phys. Rev. Lett. **82**, 2590 (1999).
[35] M. L. Brongersma, J. W. Hartman and H. A. Atwater, Phys. Rev. B **62**, R16356 (2000).
[36] S. A. Maier, M. L. Brongersma, P. G. Kik and H. A. Atwater, Phys. Rev. B **65**, 193408 (2002).
[37] S. A. Maier, P. G. Kik, H. A. Atwater, S. Meltzer, E. Harel, E., B. E. Koel and A. A.

Requicha, Nature Mat. **2**, 229 (2003).
[38] S. A. Maier and H. A. Atwater, J. Appl. Phys. **98**, 011101 (2005).
[39] D. M. Pozar, *Microwave Engineering* (Addison-Wesley, Reading, 1990).
[40] L. F. Chen, K. C. Ong, C. P. Nei, V. V. Varadan and V. K. Varadan, *Microwave Electronics* (Wiley, Chichester, 2004).
[41] K. Tachibana, Y. Kishimoto and O. Sakai, J. Appl. Phys. **97**, 123301 (2005).
[42] Y. Ito, O. Sakai and K. Tachibana, Plasma Sources Sci. Technol. **19**, 025006 (2010).
[43] D. R. Smith, D. C. Vier, Th. Koschny and C. M. Soukoulis, Phys. Rev. E **71**, 036617 (2005).
[44] S. C. Brown, *Basic Data of Plasma Physics* (MIT Press, Boston, 1959).
[45] S. S. Bedair and I. Wolff, IEEE Trans. Microw. Theory Tech. **40**, 41 (1992).
[46] O. Sakai, S. Iio, T. Shimomura and K. Tachibana, Trans. Mat. Res. Soc. Jpn. **39**, 449 (2011).
[47] S. Ancey, Y. Decanini, A. Folacci and P. Gabrielli, Phys. Rev. B **76**, 195413 (2007).

VI. Publication of results in this project

(a) Scientific papers (peer reviewed)

1. O. Sakai and K. Tachibana,
   "Plasmas as metamaterials: a review,"
   Plasma Sources Science and Technology, vol. 21, pp. 013001-1-18 (2012), Jan.
2. O. Sakai, J. Maeda, T. Shimomura and K. Urabe,
   "Functional composites of plasmas and metamaterials for flexible waveguides and variable attenuators with controllable phase shift,"
   Physics of Plasmas (submitted).
3. O. Sakai, J. Maeda, T. Shimomura and K. Urabe,
   "Overdense Microwave Plasma Generation in a Negative-Permeability Space,"
   Plasma and Fusion Research (submitted).

(b) Conference papers

1. S. Iio, K. Imanaka and O. Sakai,
   "Overdense electron density of microwave plasma in negative-permeability space,"
   Proceedings of 33rd International Symposium on Dry Process, (Kyoto, Japan, November 10-11, 2011), pp. 55-56.
2. O. Sakai Y. Nakamura and S. Iio,
   "Transition to negative refractive index in plasma metamaterial with negative permeability,"

Proceedings of The Sixth International Congress on Advanced Electromagnetic Materials in Microwaves and Optics (Metamaterials' 2012) (St. Petersburg, Russia, September 17-22, 2012) (in CD-ROM).

3. O. Sakai, (Invited)
"Novel functional composites of plasmas and metamaterials,"
The 54st Annual Meeting of the American Physical Society Division of Plasma Physics (Providence, USA, October 29 - November 2, 2012) (*Abstracts*, p. 244).

(c) Patent submission

(None)